Anisotropic Plasmonic Gold Nanorod−Indocyanine Green@Reduced Graphene Oxide−Doxorubicin Nanohybrids for Image-Guided Enhanced Tumor Theranostics

Swarup Kumar Maji, Subin Yu, Eunshil Choi, Ju Won Lim, Dohyub Jang, Ga-young Kim, Sehoon Kim,* Hyukjin Lee,* and Dong Ha Kim*

ACCESS | Metrics & More | Article Recommendations | Supporting Information

ABSTRACT: The unique physicochemical and localized surface plasmon resonance assets of gold nanorods (GNRs) have offered combined cancer treatments with real-time diagnosis by integrating diverse theragnostic modalities into a single nanoplatform. In this work, a unique multifunctional nanohybrid material based on GNRs was designed for *in vitro* and *in vivo* tumor imaging along with synergistic and combinatorial therapy of tumor. The hybrid material with size less than 100 nm was achieved by embedding indocyanine green (ICG) on mesoporous silica-coated GNRs with further wrapping of reduced graphene oxide (rGO) and then attached with doxorubicin (DOX) and polyethylene glycol. The nanohybrid unveiled noteworthy stability and competently protected the embedded ICG from further aggregation, photo-bleaching, and nucleophilic attack by encapsulation of GNRs-ICG with rGO. Such combination of GNRs-ICG with rGO and DOX served as a real-time near-infrared (NIR) contrast imaging agent for cancer diagnosis. The hybrid material exhibits high NIR absorption property along with three destined capabilities, such as, nanozymatic activity, photothermal activity, and an excellent drug carrier for drug delivery. The integrated properties of the nanohybrid were then utilized for the triple mode of combined therapeutics of tumor cells, through synergistic catalytic therapy and chemotherapy with combinatorial photothermal therapy to achieve the maximum cancer killing efficiency. It is assumed that the assimilated multimodal imaging and therapeutic capability in single nanoparticle platform is advantageous for future practical applications in cancer diagnosis, therapy, and molecular imaging.

Mesoporous silica coated Au NR loaded with ICG and wrapped with rGO for Photo- and Catalytic Therapy
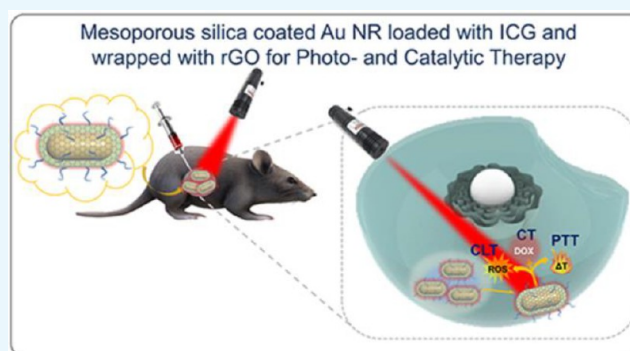
INTRODUCTION

The recent development of nanoengineered multifunctional structures in the areas of nanotechnology has engendered a great deal of interest by the worldwide scientific community, which could be possibly cast off in a clinical tactic for a concurrent merger of multidiagnostic tests and single and collective treatments, the so-called nanotheranostic devices.[1−4] The proper selection of the desired criterion features would be able to give a significant reduction in drug doses with an ensuing decrease of unfavorable side effects and fusion of more than one therapeutic treatments for enhancing the therapeutics with a real-time monitoring ability and could be very useful for the premature analysis of cancer and further life threatening diseases.[5]

The anisotropic GNRs among the several diverse gold nanostructures, have attracted much attention in cancer theragnosis owing to their exceptional optical, photothermal, and biocompatible properties.[6,7] In past few years, an extensive study has been made in various fields of applications, such as, multiphoton imaging,[8,9] photoacoustic imaging,[10,11] biosensing,[12,13] hyperthermia therapy,[14,15] drug/gene delivery,[16,17]

catalysis,[18,19] optical recording and data storage,[20,21] and image guided cancer therapy.[22,23] The most fascinating features for all these applications are based on the tunable localized surface plasmon resonance (LSPR) property, which is originated by the interactions of pacified light with the nanocrystals, which then induce powerful local field enrichment at the tips.[24] The generated enhance field could be exploited to activate drug release for chemotherapy and/or creation of reactive oxygen species (ROS) for photodynamic therapy and/or to provide hyperthermal cancer therapy.[25,26] On the other hand, indocyanine green (ICG), which is a prototypical dye with solid absorption band at about 800 nm, is a FDA approved near-infrared (NIR) active amphipathic tricarbocyanine dye for
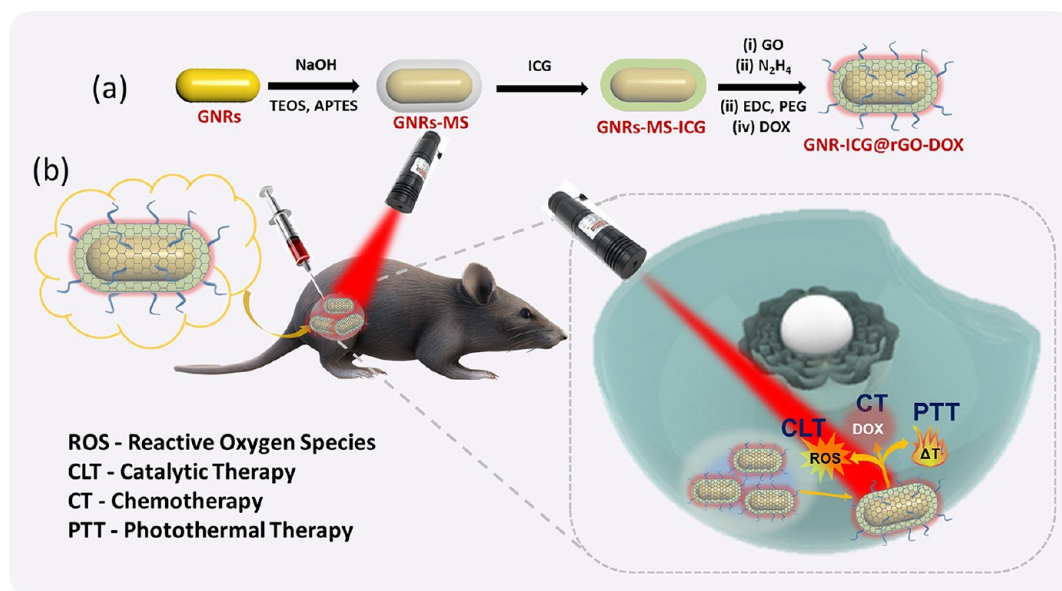
Scheme 1. (a) Schematic Illustration of the Synthetic Procedures of GNRs-ICG@rGO-DOX and (b) Schematic Illustration for Synergistic Catalytic Chemotherapy with Sequential Photothermal Therapy with 808 nm NIR Light Exposure for Enhanced Tumor Ablation

clinical applications in cancer theranostic, has been chosen to encapsulate to overcome its intrinsic drawbacks[23,27] like low quantum yield, limited photostability, rapid blood clearance in physiological conditions, and restricted availability for functionalization, which otherwise limits its further applications.[27] However, ICG has shown great potential in NIR contrast imaging and photodynamic/photothermal therapy when integrated into different nanoplatforms.[28] Although, a few studies has been made to combine the features of Au NRs with ICG,[23,28−32] however, more extensive studies are required to fully minimize the drawbacks and to get the maximum synergistic efficiency from them. Again, graphene oxide (GO) have concerned tremendous attentiveness in the areas of biomedical science for its extraordinary physiochemical properties.[33] The previous reports have been suggested that ultrathin GO could be an excellent candidate for improving the stability and efficiency of hybrid nanostructures for multiple purposes, along with a carrier for model drug as a nanovehicle for cancer therapeutics.[34] Thus, to realize novel functions of GO for biomedical purposes, the balanced strategy of a GO-based material is extremely mandatory.

In the case of the cancer diagnosis, several medical imaging techniques, along the lines of magnetic resonance imaging (MRI), computed tomography (CT), ultrasound imaging, single-photon emission computed tomography imaging, photo-acoustic imaging, positron emission tomography (PET), and fluorescence imaging (FL), have been developed for delicate and precise detection of early cancer and also previously undetectable tumors.[5] The Au NRs based nanomaterials are one of the most suitable candidates for this context of in-depth imaging capability as mentioned earlier.[9,10] In combination to the diagnosis, researchers have been developing several strategies to utilize various therapeutic procedures, viz, high intensity focused ultrasound therapy (HIFU), chemotherapy (CT), radiotherapy (RT), photothermal therapy (PTT), photodynamic therapy (PDT), magnetic hyperthermia (MHT), immunotherapy (IT), gene therapy (GT), and a recently developed catalytic therapy (CLT) for the destruction

of tumors.[5,35] Recent advances in cancer treatment proved that the collective therapy, which exploits the combination of dual or additional treatment forms, could result in enhanced therapeutic performance for complete elimination of cancer through ostentatious super additive therapeutic effects.[5,22,23] Thus, there is a huge possibility to design a multifunctional theranostic systems for image guided combination therapy for cancer theragnosis. However, development of such a multi-functional theranostic platform is of great challenge for the safety of therapeutic regimes and to optimize therapeutic efficacy.

In this work, we have invented a core@shell alike hybrid nanostructure (GNRs-ICG@rGO-DOX) consisting of meso-porous silica coated GNRs, with ICG, GO, and a model drug, doxorubicin, for image-guided synergistic therapy of cancer cells (Scheme 1b). The peroxidase-like and chemotherapeutic activity was then extensively studied under physiological conditions. The rational design was also found to be effective for enhancing generation photothermal effects under LSPR excitation and could be utilized for the utmost cancer killing efficiency.

■ MATERIALS AND METHODS

Chemicals. Gold(III) chloride trihydrate (HAuCl$_4$·3H$_2$O; ≥ 99.9%), sodium borohydride (NaBH$_4$, 99%), trisodium citrate dihydrate, hexadecyltrimethylammonium bromide (CTAB, ≥ 98%), ascorbic acid (AA), silver nitrate (AgNO$_3$, ≥ 99.0%), tetraethyl orthosilicate (TEOS, 98%), (3-amino-propyl) triethoxysilane (APTES, 99%), 9,10-anthracenediylbis-(methylene) dimalonic acid (ABDA, ≥ 90%), 3,3′,5,5′-tetramethylbenzidine (TMB, ≥ 99.0%), terephthalic acid (TA, 98%), 2′,7′-dichlorodihydrofluorescein diacetate (DCFH-DA, ≥ 97%), sodium acetate (>99%), phosphate buffered saline tablet (PBS), indocyanine green (ICG, United States Pharmacopeia reference standard), cyanine-5.5 (Cy-5.5) dye, graphite powder (99.99%), potassium permanganate (KMnO$_4$, ≥ 99.0%), hydrazine hydrate (24−26% in H$_2$O), and glacial acetic acid were procured from Sigma-Aldrich.

Sulfuric acid (H_2SO_4) and hydrochloric acid (HCl) were obtained from Daejung Chemicals & Materials Co., Ltd. Ammonia solution ($NH_3 \cdot H_2O$, 30%) was procured from Daejung Chemical. Hydrogen peroxide (H_2O_2, 30%) was procured from Junsei Chemical Co., Ltd. Doxorubicine hydrochloride (DOX, ≥ 99.9%) was procured from Futurechem Co., Ltd. DiaEasy Dialyzer MWCO 14 kDa was acquired from BioVision. 6-Arm PEG amine, HCl salt (PEG–NH_2, ≥ 95%, MW 15000) was acquired from JenKem Technology USA. N-(3-(Dimethylamino)propyl)-N′-ethylcarbodiimide hydrochloride (EDC, ≥ 98.0%) was purchased from Alfa aesar. MTT assay kit (EZ-cyTox) was bought from Daeil Lab Service Co., Ltd., Republic of Korea. The solvents were utilized as obtained.

Synthesis of GNRs-MS. GNRs were produced according to the previously reported process with certain modification.[36] Concisely, CTAB-capped Au seeds were prepared first, in which 7.5 mL of CTAB (0.1 M) was put together with 250 μL of (0.01 M) $HAuCl_4$ and then 1.65 mL of deionized (DI) water under gentle stirring. 0.6 mL of ice-cold $NaBH_4$ (0.01 M) solution was then add on to the above solution mixture. The seed solution appeared immediately and was applied within 2−5 h. The growth solution for GNRs contained of a combination of 100 mL of CTAB (0.1 M), 5 mL of $HAuCl_4$ (0.01 M), 0.8 mL of $AgNO_3$ (0.01 M), 2 mL of H_2SO_4 (0.5 M), and 800 μL of ascorbic acid (0.1 M). The growth reaction was begun by the inclusion of 240 μL of seed solution, and the reaction was carried on for 15 h at 30 °C in the process of gentle stirring.

GNRs were then coated with mesoporous silica ($mSiO_2$) according to the well-established method with slight modification.[22] Briefly, 20 mL of synthesized GNRs was centrifuged (6000 rpm, 15 min, once) and then the residue was diluted to 10 mL by adding DI water. Then, 100 μL of NaOH (0.1 M) solution was put on upon gentle stirring. After 5 min, following this period, two successive additions of 30 μL of 20% TEOS (in methanol) was done under mild stirring at 30 min breaks. In the last step, 30 μL of 20% TEOS with 30 μL of 20% APTES were mixed into the reaction mixture and permitted to react for 24 h at ∼28 °C. GNRs-MS was then accumulated by centrifugation followed by cleaning with ethanol for various times.

Loading of ICG to GNRs-MS. First, 2.5 mL of ICG (12 μg/mL, methanol) was mixed with a methanolic solution of 10 mL of GNRs-MS and reacted for 6 h at room temperature under a dark condition with gentle stirring and sonication. The GNRs-ICG nanocomposite was collected by centrifugation and washing through ethanol and water for three times.

Synthesis of GNRs-ICG@rGO. GO sheets were produced by the modified Hammer method. The large GO sheets were then converted to nano-GO sheets (NGO) by probe sonication at 500W for 2h and collected by filtration through a 400 nm syringe filter.[34]

To synthesize NGO encapsulated GNRs-ICG, 1 mL of aqueous solution of GNRs-ICG was mixed into 5 mL of NGO solution (0.05 mg/mL) under bath sonication. The suspension was vortexed for 6 h at ambient temperature to complete the electrostatic interaction process. After that 10 μL of NaOH and 50 μL of hydrazine (35%) were mixed with above suspension and heated for 2−5 min at 80 °C to convert GO to rGO. The GNRs-ICG@rGO was accumulated by centrifugation and washing with water for three times and finally filtered through 400 nm syringe filter.

Synthesis of GNRs-ICG@rGO-PEG. Four mg of EDC was mixed into 1 mL of the above synthesized GNRs-ICG@rGO aqueous solution and stirred for 5 min. Twenty-five mg of 6-arm PEG amine was mixed, and the reaction was continued for 2 h.[38] The GNRs-ICG@rGO-PEG was accumulated by centrifugation and washing with water.

Synthesis of GNRs-ICG@rGO-DOX. In 1 mL of GNRs-ICG@rGO-PEG aqueous solution, 50 μL of DOX (1 mg/mL) was added under stirring and continued overnight at room temperature in dark. The GNRs-ICG@rGO-DOX nanohybrid was accumulated by centrifugation and washing with water. The GNRs-ICG@rGO-DOX was also combined with a NIR dye Cy-5.5 in a similar way as that of DOX attachment to get the GNRs-ICG@rGO-DOX@Cy-5.5 hybrid material.

Nanozymatic Activity. The peroxidase-like catalytic activity (POD) were measured in 3 mL of (0.1 M, pH 4.5) acetate buffer solution with 13 mM H_2O_2, 0.5 mM TMB, and GNRs-ICG@rGO (100 μL) at 37 °C. After 10 min, an aliquot was withdrawn and collected, and the absorbance spectrum was measured by a UV−vis spectrophotometer. The controlled experiments were also carried out in the absence of either H_2O_2 or GNRs-ICG@rGO.

Photothermal Activity. One mL of aqueous solutions of PBS, ICG (4 μM), GNRs-MS (1 nM), GNRs-ICG (1 nM) and GNRs-ICG@rGO-DOX (1 nM) were exposed with 808 nm NIR laser (CW, 2 W/cm^2) for 15 min. The temperature changes were monitored at certain times by a thermocouple. The photothermal stability of ICG and GNRs-ICG@rGO-DOX were measured by the three successive on/off cycle of 808 nm NIR laser (2 W/cm^2).

Drug Release in PBS. First, 0.5 mL of GNRs-ICG@rGO-DOX was suspended in 1 mL of PBS under three different pH of 7.4, 6.0, and 4.5 and then mild stirred at 37 °C for 24 h. At certain time intervals (first 2 h and then 4 h), an aliquot part of the solution was collected and centrifuged. The released DOX amount was measured from the supernatant by the UV−vis spectrophotometer.

Characterization. Transmission electron microscopy (TEM) pictures were collected with a Tecnai G2 20 S-TWIN TEM. Scanning electron microscopy (SEM) pictures were obtained by a JEOL JSM6700-F. Raman spectra were recorded by a LabRamHREvo 800 (HORIABA JobinYvon, France). UV−vis−NIR absorbance spectra were measured on a Varian Cary5000 spectrophotometer. Fluorescence spectra were acquired by using a PerkinElmer LS 55 spectrofluorimeter. Fourier-transform infrared (FTIR) spectroscopic measurements were conducted with a Varian 800 FT-IR. The ζ potentials were measured on a Malvern Zetasizer Nano ZS.

FDTD Simulation. The finite-difference time-domain (FDTD) simulation method was performed by Lumerical Solutions using FDTD Solutions 8.6. The electromagnetic pulse of 780 nm was applied to excite the target nanostructure. The refractive index of water of 1.33 was set as the surrounding medium. The periodic boundary with 0.5 nm of mesh size settings for the x-axis and y-axis was utilized though appropriately matched layer condition for the z-axis and was exerted to engage all light propagating to the outward. The optical constants of Au, SiO_2, ICG, and rGO were obtained from Johnson, Christy and Palik, and previous literature.[37] The sizes of the nanocomposites and hybrid were considered from the average sizes obtained through TEM images.

Cell Culture. Human colon cancer (HT-29) cells were matured at 37 °C with 5% CO_2 in Dulbecco's Modified Eagle's
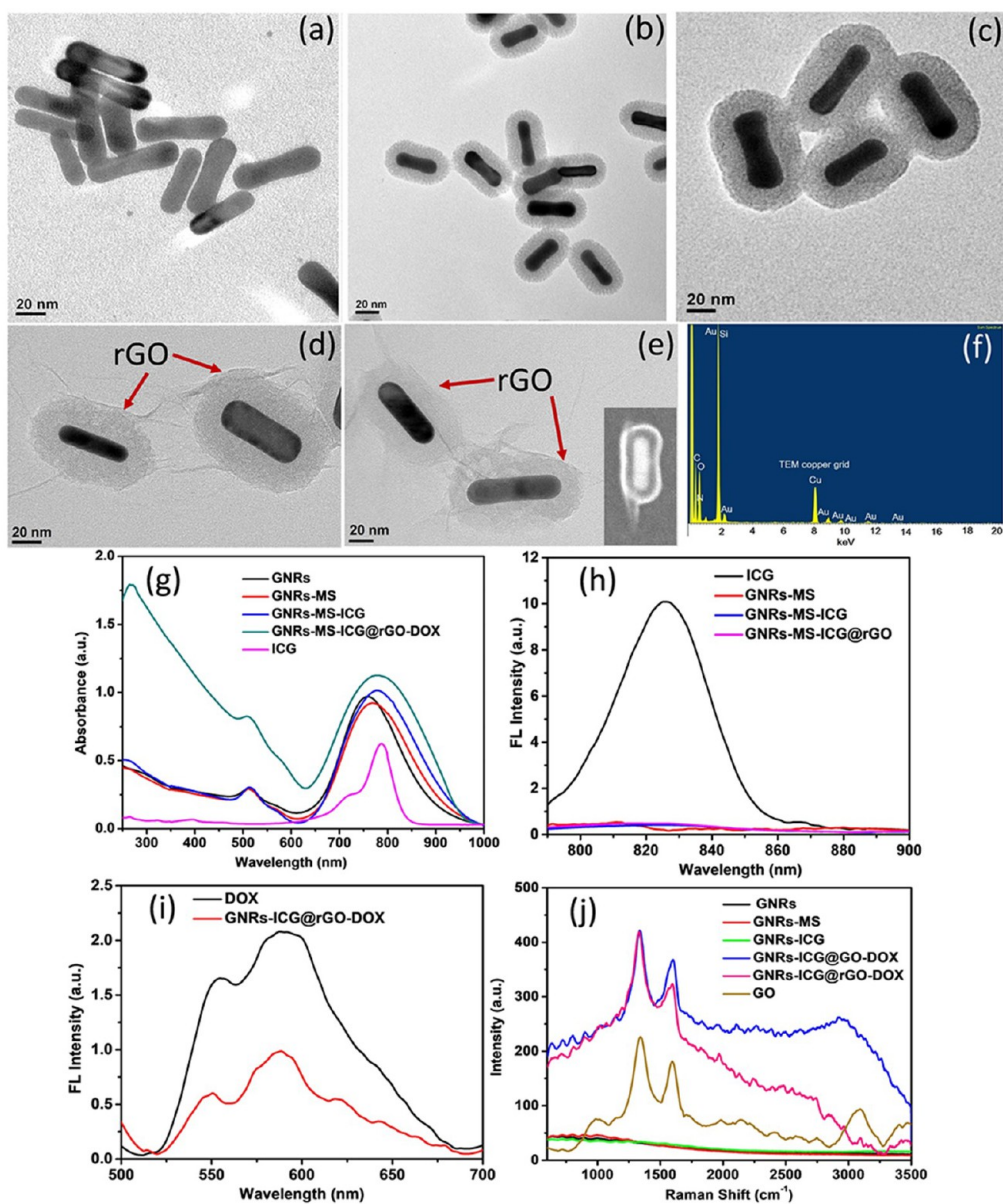
Figure 1. Structural and Spectroscopic Characterizations. TEM images of (a) GNRs, (b) GNRs-MS, (c) GNRs-ICG, (d) GNRs-ICG@rGO, and (e) GNRs-ICG@rGO-DOX (inset: FESEM image). (f) EDX spectrum of GNRs-ICG@rGO-DOX. (g) UV–vis–NIR absorbance spectra of ICG, GNRs, GNRs-MS, GNRs-ICG and GNRs-ICG@rGO-DOX. (h) Fluorescence spectra of ICG, GNRs-MS, GNRs-ICG, and GNRs-ICG@rGO-DOX. (i) Fluorescence spectra of DOX and GNRs-ICG@rGO-DOX. (j) Raman spectra of GNRs, GNRs-MS, GNRs-ICG, GNRs-ICG@GO–DOX, GNRs-ICG@rGO-DOX, and GO.

Medium (DMEM) supplemented with 10% (v/v) fetal bovine serum, penicillin (100 U/mL), and streptomycin (100 mg/mL).

***In Vitro* Cell Imaging.** HT-29 cells were planted in DMEM onto a plastic bottomed μ-dishes, chambered cover glass (density 1×10^5 cells per dish) for 24 h. The cells were treated with GNRs-ICG@rGO, GNRs-ICG@rGO-DOX, and GNRs-ICG@rGO-DOX@Cy-5.5 (100 μg/mL) in the dark at 37 °C for 6 h. Then the cells were fixed with 4.0% formaldehyde and the slides for imaging were prepared. In the case of ROS detection in cells, after being treated with DOX, GNRs, GNRs-ICG, GNRs-ICG@rGO, and GNRs-ICG@rGO-DOX (100 μg/mL) for 6 h, DCFH-DA (20 μm) was also mixed and further incubated for 20 min. Two-photon confocal laser scanning microscopy pictures of GNRs-ICG@

rGO were acquired using a Leica TCS SP5X multiphoton microscope. Confocal laser scanning microscopy pictures were taken with a Nikon D-Eclipse C1 fluorescence microscope.

The viable and dead cells staining by CLSM images of HT-29 cells were conducted by incubating into a plastic bottomed μ-dishes with chambered cover glass. The viable and dead cells were visualized after cytotoxicity experiments under different conditions, and two staining reagents 3′,6′-di(O-acetyl)-4′,5′-bis[*N*,*N*-bis(carboxymethyl)aminomethyl]fluorescein, tetraacetoxymethyl ester (calcein-AM) and propidium iodide (PI) were employed to stain viable cells by means of green fluorescence (λ_{ex} = 490 nm, λ_{em} = 515 nm) and expired cells as red fluorescence (λ_{ex} = 535 nm, λ_{em} = 617 nm). After the removal of DMEM and washing of the disks, 100 μL of calcein-AM (20 mM) and 100 μL of PI (20 mM) solutions were

added and after 15 min, staining solution were drawn out and further washed with PBS. Now the samples are ready for subsequent visualization through CLSM.

***In Vitro* Cell Viability.** The HT-29 cells were grown into 96-well plates at a density of 5×10^4 cells/well and incubated with different samples, such as DOX, GNRs-ICG, GNRs-ICG@rGO, and GNRs-ICG@rGO-DOX (0−300 μg/mL) at 37 °C. After 24 h in dark, the selected wells were exposed to an 808 nm continuous-wave diode laser (Hi-Tech Optoelectronics Co. Ltd.) with a power density of 2 W/cm^2 for different times. After NIR light illumination, the old DMEM was substituted with fresh DMEM and the cells further cultured for 24 h. The percentage of cell viability was estimated employing an Infinite M200 PRO micro plate reader. A normal cell human embryonic kidney 293 cells (HEK-293) were also grown and tested similarly with GNRs-ICG@rGO.

***In Vivo* Animal Experiments.** Animal trials were conducted in agreement with the KIST (approval number: KIST-2020−073). 5-week-old male BALB/c mice were procured from Nara Biotech (Korea). To establish the HT-29 xenograft tumor model, mice were injected subcutaneously with 1×10^7 HT-29 and waited for tumors grow to ~100 mm^3. The real-time NIR fluorescence pictures of the tumor region in mice were documented at different times after the peritumoral injection of GNRs-ICG@rGO-DOX@Cy-5.5 (400 μg/mice) by using an IVIS Spectrum imaging system (λ_{ex} = 640 nm, and λ_{em} = 710 nm). Infrared thermal images of HT-29 tumors were acquired after 1 h post injection of materials by an infrared thermal imaging camera (FLIR-E6390), with irradiation for 10 min through 808 nm laser light of 2 W/cm^2.

For therapeutic purposes, the HT-29 tumor bearing mice were allotted to two groups (n = 3 mice/group) for two different treatments. Mice were peritumorally injected with (i) PBS as control (400 μg/mice), and (ii) GNRs-ICG@rGO-DOX@Cy-5.5 (400 μg/mice) and then followed by NIR laser illumination (808 nm, CW, 2 W/cm^2) for 10 min after 1 h post injection. The tumor size was measured every day by using a digital vernier caliper. The tumor volumes were calculated by the following equation: volume = (tumor length) × (tumor width)^2/2. The relative tumor volume was normalized with the initial size before administration.

■ RESULTS AND DISCUSSION

Synthesis and Characterization. The overall synthetic progression for the preparation of GNR-ICG@rGO-DOX is depicted in Scheme 1a and the digital photographs of GNRs, GNRs-MS, GNRs-ICG, and GNRs-ICG@rGO-DOX are shown in Figure S1. As revealed in the TEM image in Figure 1a, the mean length and width of GNRs was shown to be 14 and 55 nm, respectively (Figure S2a). After coating of thick mesoporous silica layer (~30 nm) on GNRs, the overall length and width was increased to 57 and 88 nm, respectively (Figure 1b and Figure S2b). The TEM image in Figure 1b also revealed the formation of well-defined mesopores of ~5 nm in silica shell on the Au core, whereas, after the loading of ICG into the mesoporous channels of SiO$_2$, the mesopores were not observed and the size of the nanocomposite was remained same as the case of GNRs-MS (Figure 1c and Figure S2c). The TEM image of rGO coated GNRs-ICG is shown in Figure 1d. A thin rGO layer was clearly observed with the thickness of ~2 nm, and the overall size of the nanocomposite also remained same after the modification of PEG and DOX (Figure 1e and Figure S2d) (width ~60 nm and length ~90 nm). The hybrid

material was also characterized by the SEM image capture (Figure 1e inset) and was in good agreement with the TEM analyses. The FTIR spectra analyses and zeta potential (ζ) measurements were also conducted to monitor the stepwise formation of nanocomposites and hybrid material (Figures S3 and S4), where the results were in good agreement with previous reports to support our experimental findings. The UV−vis−NIR absorbance spectrum of GNRs showed the longitudinal LSPR maximum at 758 nm, which was red-shifted to 768 nm after mSiO$_2$ coating (Figure 1g). After loading of ICG (Figure 1g), the LSPR peak of GNRs-MS was again red-shifted to 780 nm with an obvious enhancement in peak intensity, which confirmed the successful loading of ICG. The loading of ICG was also confirmed by the decrease in absorbance intensity before and after loading into GNRs-MS (Figure S5a). The LSPR peak was further obviously enhanced with the rGO wrapping due to the plasmonic effect and light absorption property.[34,39] The wrapping of rGO on GNRs-ICG was also confirmed by the appearance of signature peak at ~270 nm for rGO.[34] The fluorescence spectra were recorded to characterize the composite and hybrid material and are shown in Figure 1h. The strong emission peak for pure ICG in methanol was obtained at ~820 nm under the excitation of 785 nm. The emission peak of ICG was almost disappeared (~99% quenching) when loaded into the mesoporous silica shell and also after coated with rGO and the fluorescence quenching is ascribed to the nanoparticle surface energy transfer (NSET) effect[23] and dye self-aggregation.[40] The fluorescence quenching could convert into photothermal conversion by nonradiative decay and consequently to an increase of the photothermal activity.[23,40] The fluorescence false-color pixel intensity maps was also monitored (Figure S6a) and any kind of fluorescence signal was not detected in the case of GNRs, GNRs-MS, GNRs-ICG, and GNRs-ICG@rGO-DOX in water under an excitation of 785 nm. The confirmed aggregation followed by fluorescence quenching could be greatly beneficial to increase the photo and thermal stability and further improve ICG-based PTT. The loading of DOX in the hybrid material was then confirmed by the fluorescence spectral measurements and the signature emission peaks were observed at 550 and 590 nm in the case of GNRs-ICG@rGO-DOX (Figure 1i). The change in absorbance spectra of the hybrid material before and after loading also confirmed the successful loading (loading capacity = 31.89%) of DOX (Figure S5b). The fluorescence false-color pixel intensity maps were also measured under the excitation of 485 nm, and a bright fluorescence was detected for the GNRs-ICG@rGO-DOX due to the presence of DOX in the hybrid (Figure S6b). The Raman spectral analysis was conducted to further characterize the nanocomposites and final hybrid material and is shown in Figure 1j. The D and G band for rGO only appeared in the case of GNRs-ICG@rGO-DOX hybrid at 1330 and 1600 cm^{-1}, respectively, whereas, the conversion of GO to partially reduced GO was also monitored by the change in intensity ration between them (I_D/I_G value 1.14 was increased to 1.29).[34,39] Furthermore, one of the major issues in the case of stability of the nanohybrid system in biological condition and under laser irradiation were fully studied and a promising outcome was noticed from our experimental observations (see the Supporting Information and Figures S7−S9).

Nanozymatic Activity. After complete characterization, the nanozymatic property of the GNRs-ICG@rGO hybrid was
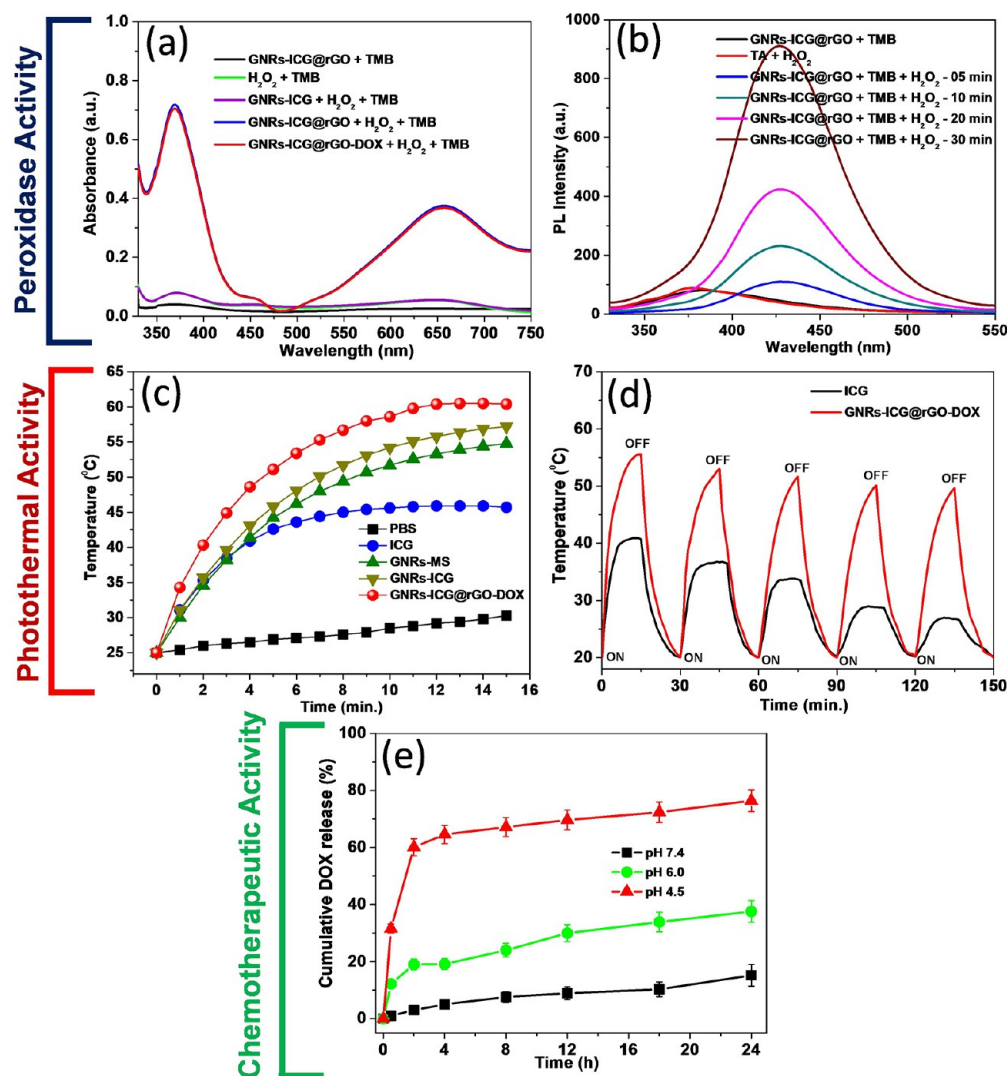
Figure 2. Multimode activity toward therapy. Peroxidase activity of GNRs-ICG@rGO: (a) UV−vis−NIR absorbance spectra of TMB solution (0.5 mM) and (b) PL spectra of TA solution (6×10^{-3} M) in 0.01 M PBS (pH = 4.0, 40 °C) with the presence/absence of GNRs-ICG@rGO and with/without H_2O_2 (13 mM) at different times. Photothermal activity of GNRs-ICG@rGO: (c) Photothermal heating curves of different samples of NIR laser exposure (808 nm, CW, 2 W/cm^2) and (d) temperature change of pure ICG and GNRs-ICG@rGO-DOX aqueous solution over five laser ON/OFF cycles under identical conditions. Chemotherapeutic activity of GNRs-ICG@rGO-DOX: (e) cumulative release profile of DOX from GNRs-ICG@rGO-DOX nanohybrid in PBS at pH 7.4, 6.0, and 4.5 at 37 °C.

first explored by the evaluation of the intrinsic POD property by the way of peroxidase substrate 3,3′,5,5′-tetramethylbenzidine (TMB) oxidation in the occurrence of H_2O_2.[41−46] In this reaction, TMB could be oxidized to ox-TMB in the presence of H_2O_2 and GNRs-ICG@rGO and would be easily visualized by the naked eye with the formation of a blue color product.[41] The color generation reaction was observed by the UV−vis spectroscopic measurements and are shown in Figure 2a under different reaction conditions. Comparable to that of the natural enzyme horseradish peroxidase (HRP),[41] two well-resolved representative peaks (for ox-TMB) were obtained at 370 and 652 nm, respectively, when the reaction mixture contained TMB, H_2O_2, and GNRs-ICG@rGO in 0.1 M PBS (pH ∼ 4, 37 °C). In contrast, no apparent color formation was noticed in the case of controlled experiments, i.e., in the absence of GNRs-ICG@rGO, the other one without H_2O_2 under identical reaction conditions (Figure 1a). The POD test was also performed correspondingly with GNRs-ICG@rGO-DOX,

and a similar spectrum was also obtained as that of GNRs-ICG@rGO. Thus, the color generation result indicated the superior peroxidase-like/nanozyme/catalytic property of the GNRs-ICG@rGO hybrid in acidic condition. The most suitable mechanism for POD activity has been extensively studied in previous reports and established that the *in situ* generated ROS on rGO surface are the main counter parts for this conversation.[41−45] The *in situ* generation of hydroxyl radicals ($^•$OH) was demonstrated by the photoluminescence probing technique of terephthalic acid (TA).[41,46] Initially, the controlled experimentations were conducted in 0.1 M PBS (pH ∼ 4, 37 °C) with TA solution (6×10^{-3} M) giving either the occurrence of H_2O_2 or GNRs-ICG@rGO hybrid, in which no well-defined fluorescence peak formation at 435 nm was obtained (Figure 2b). However, as shown in Figure 2b, the nonluminescent TA was transformed to a luminescent 2-hydroxy-TAby reacting with $^•$OH with an emission peak cantered at 435 nm in occurrence of both H_2O_2 and GNRs-

ICG@rGO. It is interesting to see that the emission peak intensity was increased linearly with time of incubation, suggesting greater generation of OH with the progress of the reaction.

Plasmon-Enhanced Photothermal Property. Due to the enhanced NIR absorption, the photothermal property of GNRs-ICG@rGO nanohybrid was then anticipated under NIR light irradiation for 15 min (808 nm, CW, 2 W/cm^2) (Figure 2c). A very negligible temperature variation was observed in the photothermal heating curve for PBS, whereas a noticeable temperature variation from room temperature (25 °C) to a maximum temperature of 45.7 °C was obtained for the pure ICG solution, which is also a widely used photothermal treatment agent.[23,47] As expected, the GNRs-MS and GNRs-ICG both induced a prominent temperature increase from room temperature to 54.8 and 57.2 °C in 15 min, respectively, and the trend is well matched with previous reports.[23] The increasing trend in photothermal property from GNRs to GNRs-ICG could be elucidated by the loading of ICG in GNRs-MS followed by the fluorescence quenching and a synergistic plasmonic effect was obtained, since both GNRs and ICG are well-known photothermal agents.[23,40] In contrast, the final hybrid material (GNRs-ICG@rGO) showed the strongest photothermal effect and the maximum temperature of 61.7 °C could be achieved with in 15 min (∼12% enhancement), which is attributed to the successful wrapping of another photothermal agent rGO on the surface of GNRs-ICG and leads to a strong plasmonic coupling.[39] The obtained photothermal heating effect from GNRs-ICG@rGO nanohybrid is suitable enough for promoting the thermal damage of cancer cells and thus might be a capable candidate for photothermal therapy. The photothermal stability and reproducibility of the GNRs-ICG@rGO was also tested and compared with those of pure ICG solution. As shown in Figure 2d, the photothermal heating curve was remained same even after five successive cycles of heating and cooling for the GNRs-ICG@rGO. On the other hand, the photothermal heating curve was markedly reduced for the case of pure ICG during the cycles of heating and cooling due to its major photobleaching and stability issues.[47] The photostability of the GNRs-ICG@rGO was also supported by the respective digital photographs without changing any color and with no change in UV−vis absorbance spectra before and after the NIR light illumination (Figure S10a), suggesting the excellent photostability of GNRs-ICG@rGO. However, a noticeable color change from green to almost colorless with significant change in UV−vis spectrum was observed for the pure ICG solution under the same condition (Figure S9b).[47]

Drug Loading and Releasing Activity. It has now been well established that GO-based materials are also excellent candidate for drug loading as well as a drug carrier.[34] In our work, the DOX molecules was successfully attached on the surface of rGO in order to get multitherapeutic modes form a single material.[34] The DOX molecules were attached to the rGO surface through π−π staking interaction and also hydrogen bond formation.[34,48,49] The cumulative DOX release behavior was then explored by incubating GNRs-ICG@rGO-DOX in PBS (0.01 M) under three different pH varied from neutral to acidic of 7.4, 6.0, and 4.5 at 37 °C, as the cellular atmosphere of maximum cancer cells is rather acidic.[34] As shown in Figure 2e, an obvious higher released amount (∼90%) with the faster release rate of DOX was observed in acidic pH (6.0, and 4.5) within 24 h, which were in good

promise with the earlier reports for GO-based materials as a drug carrier.[34] The excellent release behavior profile of DOX was obtained due to the losing strength of both the bonds through protonation in acidic condition and thus the solubility of DOX could also be increased.[48,49] The enhanced pH dependent release rate is the critical factor for drug delivery into cancer cells. It was also established that the cumulative release of DOX could further be enhanced by NIR light illumination due to the heat-simulative dissociation of π−π staking interaction.[48]

FDTD Simulation Study. The enhanced light absorbance and photothermal properties were supported by exploitation an orthogonal approach and the FDTD simulation technique was performed to estimate the electromagnetic (EM) field distributions and enhancements. The EM fields were strongly spread almost all over the GNRs in the case of GNRs-MS and GNRs-ICG, and the extreme peak intensity of the improved EM fields ($|E/E_0|^2$) was amplified from 40.1 to 46.2 after loading of ICG (integrated E field density of 122413.5 and 125090.5, respectively), which is in support to the enhanced light absorbance and photothermal activity of GNRs-ICG (Figure 3, parts a and b). It was noticed that the LEF effect
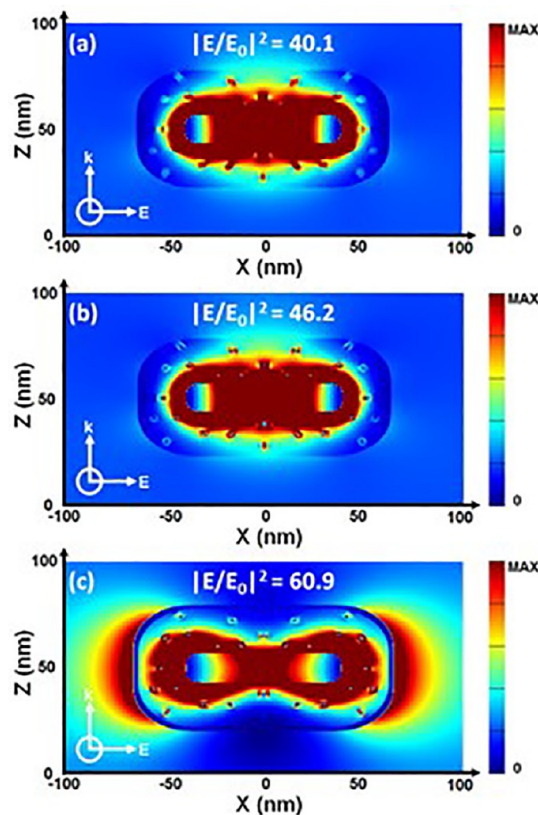

Figure 3. FDTD simulations and local field improvement of (a) GNRs-MS, (b) GNRs-ICG, and (c) GNRs-ICG@rGO-DOX, obtained under an incident excitation wavelength of 780 nm.

reduced gradually from the surface of GNRs in the direction of the outside of silica shell and thus the loaded ICG could easily experience the LEF effect (Figure S10). The EM fields distribution in GNRs-ICG@rGO was quite different compared to that of GNRs-MS and GNRs-ICG, in which EM fields were strongly spread at both ends of GNRs core and designated "hot spots" were also generated at the interfaces between GNRs-
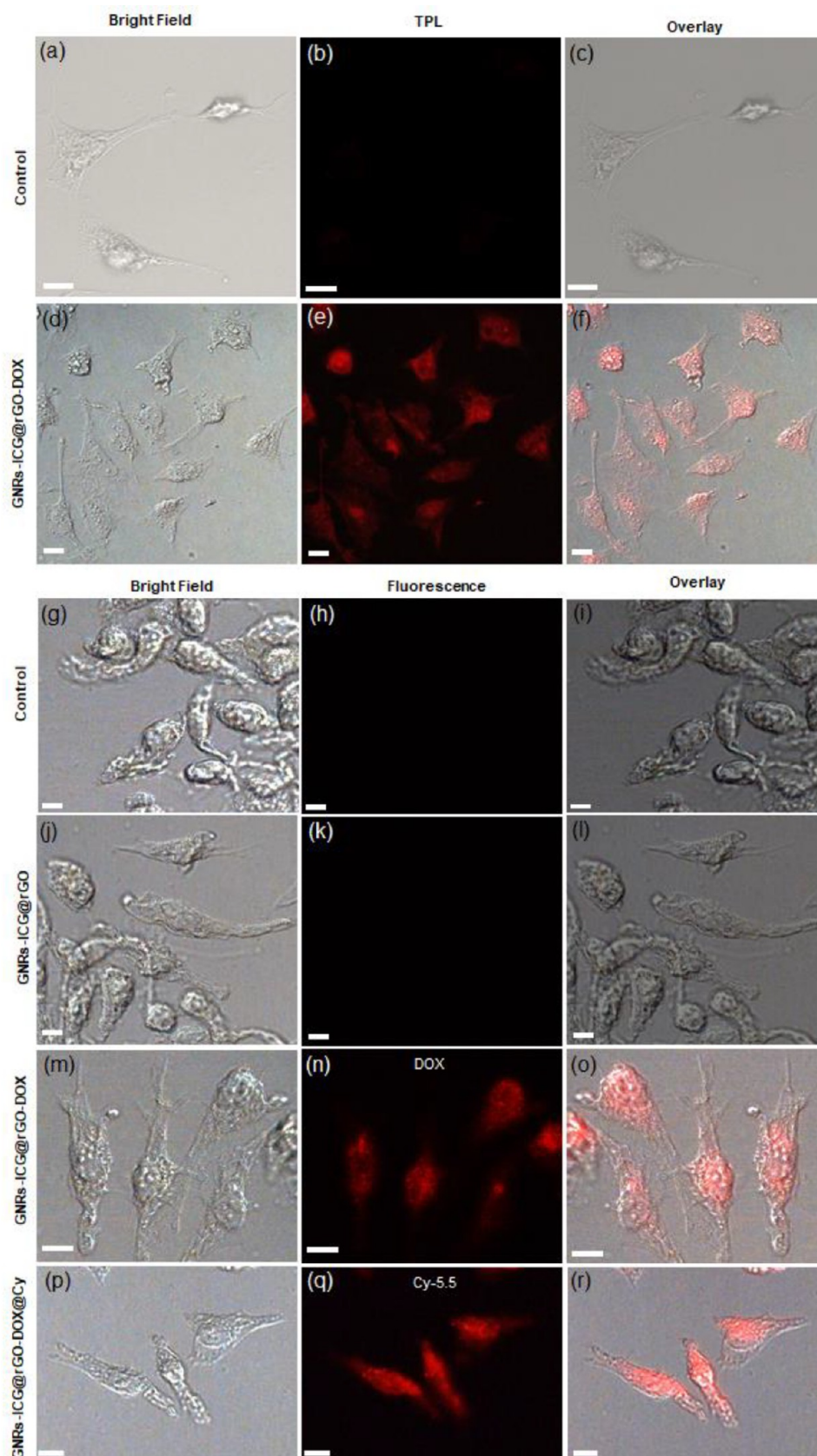
Figure 4. *In vitro* cellular localization. TPL microscopy images of HT-29 cells (a−c) as control and (d−f) as treated with GNRs-ICG@rGO-DOX (100 μg/mL) for 6 h. CLSM image of HT-29 cells (g−i) as control and as treated with (j−l) GNRs-ICG@rGO (100 μg/mL), (m−o) GNRs-ICG@rGO-DOX (100 μg/mL), and (p−r) GNRs-ICG@rGO-DOX@Cy-5.5 (100 μg/mL) (scale bar = 10 μm).
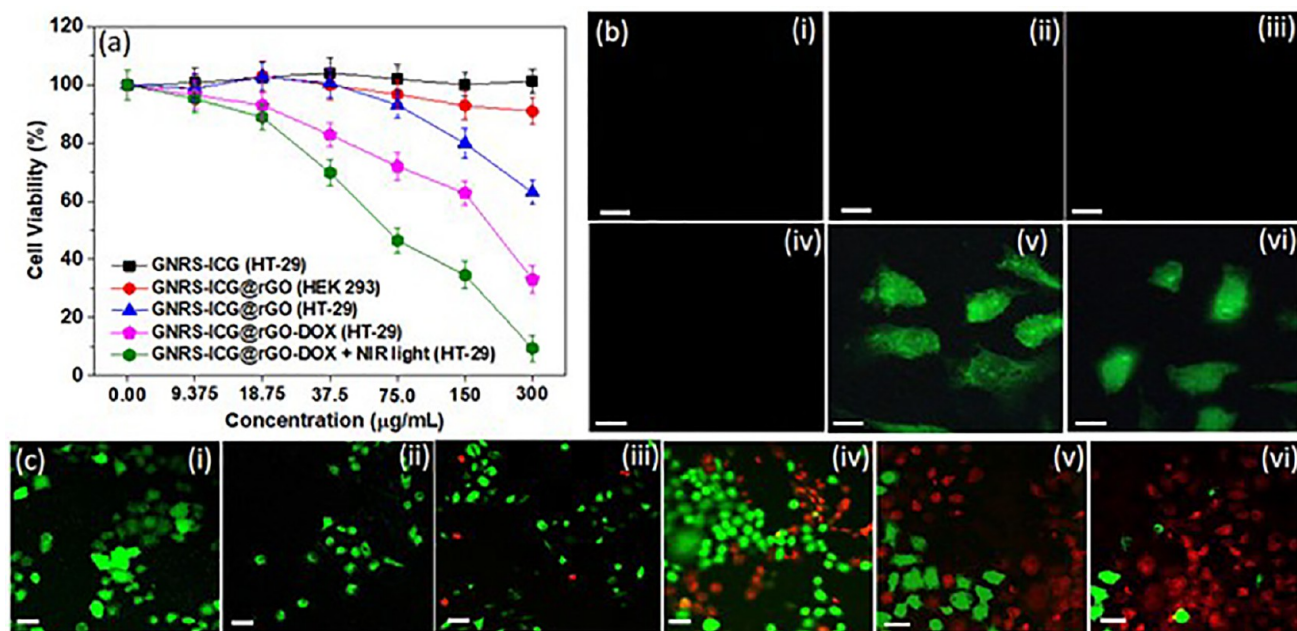
Figure 5. *In vitro* therapeutic performance. (a) Cell viability tests by MTT assay of HT-29 cancerous cells incubated with GNRs-ICG, GNRs-ICG@rGO, GNRs-ICG@rGO-DOX, and GNRs-ICG@rGO-DOX with laser exposure (808 nm, CW, 2 W/cm^2, 10 min) (0−300 μg/mL) and HEK-293 normal cells incubated with GNRs-ICG@rGO. (b) CLSM image of HT-29 cells (i) as control; as treated with (ii) DOX, (iii) GNRs, (iv) GNRs-ICG; and (v) GNRs-ICG@rGO and (vi) GNRs-ICG@rGO-DOX (300 μg/mL) followed by NIR light exposure (808 nm, CW, 2 W/cm^2) of 10 min and incubated with DCFH-DA (20 μm) (scale bar = 10 μm). (c) CLSM image of HT-29 cells costained by Calcein AM and PI in different treatment conditions (i) as control, (ii) as GNRs-ICG, (iii) DOX, (iv) GNRs-ICG@rGO, (v) GNRs-ICG@rGO-DOX, and (vi) GNRs-ICG@rGO-DOX followed by NIR light exposure (808 nm, CW, 2 W/cm^2) of 10 min (scale bar = 50 μm).

ICG and rGO in a longitudinal direction. Thus, the EM fields were further enhanced ∼1.5 times ($|E/E_0|^2 = 60.9$, integrated E field density = 152049.3) after coating with the rGO on the GNRs-ICG surface (Figure 3c), due to excellent thermal conductivity of rGO followed by the plasmonic coupling between them,[43] which also supported our experimental results. The prominent improvement in EM field intensity highlights the significance of the efficient light absorption property of GNRs-ICG@rGO for gaining improved photothermal effects and could also be an effective material for enhanced photoacoustic wave generation.[39,40]

***In Vitro* Cellular Localization and Antitumor Efficiency.** The effective endocytosis followed by localization through passive diffusion of the GNRs-ICG@rGO-DOX in tumor cells was first investigated *in vitro* by incubating with human colon cancer HT-29 for image guided multimode therapy. As shown in Figure 4, related to that of raw control cells (Figure 4a−c), bright red TPL in the dark field and in the overlay image was clearly observed inside the cell cytoplasm after incubation of 6 h with the used dose of 100 μg/mL (Figure 4d−f). The generation of bright red TPL was due to the presence of GNRs as a core material in the hybrid,[9] as well as the presence of ICG in proper position, and has been previous established the TPL enhancement for in-depth contrast imaging.[50] The successful internalization of GNRs-ICG@rGO-DOX and then the pH-dependent drug release phenomenon was also established by the CLSM image capture. As shown in Figure 4m−o, the red colored DOX fluorescence was detected in the CLSM images inside the cells after 6 h of incubation compared to that of two controlled conditions as blank (Figure 4g−i) and with GNRs-ICG@rGO (parts j−l). In addition, to obtain the multimodal imaging capability from the nanohybrid, GNRs-ICG@rGO-DOX was also attached with an

excellent NIR fluorescence dye Cy-5.5, and an obvious NIR fluorescence was also obtained in CLSM images through the bright red color generation as shown in Figure 4p−r. The GNRs-ICG@rGO-DOX@Cy-5.5 was characterized by generation of a signature fluorescence peak of Cy-5.5 at 710 nm and fluorescence false-color pixel intensity map (Figure S11). Thus, the *in vitro* cellular uptake efficiency and multimode bioimaging capability of GNRs-ICG@rGO-DOX@Cy-5.5 nanohybrid was established through NIR fluorescence and TPL imaging techniques.

The *in vitro* dark toxicity of GNRs-ICG@rGO was then examined with HT-29 cancer cells after 24 incubations for further study of the image-guided combined therapeutics. The MTT assay was performed to test the viability of HT-29 cells as controlled (Figure 5a, black line with square symbol) and treated with deferent concentration of GNRs-ICG@rGO varying from 0 to 300 μg/mL. As shown in Figure 5a, the negligible influence in cell viability was obtained up to 37.5 μg/mL of dose and almost 90% cells were viable, while the cell viability was significantly reduced in a dose-dependent manner to 63% in the case of highest dose of 300 μg/mL (blue line with trigonal symbol). The dose-dependent cell viability phenomenon is the usual trend in nanotherapeutics, and one that could easily be considered as the inherent toxicity of the hybrid material and the dose above the 100 μg/mL is not suitable for further studies. However, beyond to the as-usual characteristic and developed applications of GO in biomedical fields, we were speculating on the above observed toxicity behavior by a newly discovered inherent characteristic of the nanozymatic/peroxidase-like property of GO-based materials.[42−46] Very recently, Fiorillo et al. in their revolutionary report have shown that the GO can target cancer stem cells and could be very useful for implications for nontoxic cancer

treatment in nanotheraputics.[51] Some other reports has also been made based on this toxicity of GO in cancer cells;[52,53] however, the proper reasoning and in detail study have not been extensively done yet. In our work, as speculated, we were thoroughly investigated the peroxidase-like activity of GNRs-ICG@rGO and the generation of ROS was also proved, which is mentioned in the above sections. Thus, the decreased cell viability (63%) at high concentration is now named as catalytic therapy (CLT) and could be ascribed due to the POD activity of GNRs-ICG@rGO, in which the improved catalytic production of ROS from O_2 and overexpressed H_2O_2 in cancer cells in acidic condition is the critical factor.[41−46] The cytotoxicity of GNRs-ICG@rGO was also then experimented upon with a normal cell line HEK-293, in which no such noticeable cell death was obtained by the GNRs-ICG@rGO up to maximum dose of 300 μg/mL (Figure 5a, red line with circle symbol). Thus, indicated that the GNRs-ICG@rGO hybrid nanosystem is not toxic toward normal cells but, however, showed noticeable cell viability to 63% in the case of a cancer cells. This result also supported our speculation regarding the POD activity of the nanohybrid system inside the cancer cells due to production of excess ROS in acidic condition, thus resulting in significant cell death. The enhanced production of ROS inside HT-29 cells was also investigated by DCFH-DA fluorescence probing to support our experimental results. As shown in Figure 5b, the rapid generation of green fluorescence of DCFH-DA was detected inside the HT-29 cells in the CLSM images, when incubated with GNRs-ICG@rGO and also followed by NIR light exposure (Figure 5b, parts v and vi). Compared to the control experiments with GNRs, DOX, and GNRs-ICG (Figure 5b, parts i−iv), the generated green fluorescence indicated the higher level of ROS inside the cells[43] and thus confirmed the pronounced ability of GNRs-ICG@rGO to encourage ROS-induced cell death.[42−46]

It was noticed that the GNRs-ICG@rGO hybrid is also an excellent drug carrier and helps with fast pH modulated drug release, and the additional chemotherapeutic (CT) activity with CLT in HT-29 cells was then performed to achieve the higher therapeutic efficiency. In this case, HT-29 cells were incubated with 300 μg/mL of GNRs-ICG@rGO-DOX. As it was tested, the very fast pH responsive release of DOX from the hybrid material in acidic condition (Figure 2e) showed that then the released DOX could easily enter the nucleus by preventing the replication of nucleic acid for killing the cancer cells by prompting cell apoptosis.[34] As shown in Figure 5a, the cell viability was then found to drop pronouncedly from 63% to ∼33% by incubating with GNRs-ICG@rGO-DOX with same material concentration (300 μg/mL) (Figure 5a, pink line with pentagon symbol). The combine and synergistic CLT and CT were the reason behind the obtained cell death phenomenon by GNRs-ICG@rGO-DOX. The cell viability test by MTT assay was also obtained for free DOX in which significant amount of cell killing phenomenon could be noticed due to anticancer property by DOX (Figure S12b). Thus, the excellent drug carrier potentiality of GNRs-ICG@rGO was proved and could be more advantageous for drug delivery in cancer therapeutics by considering the potential side effect for treatment with free DOX.

The potential photothermal activity of GNRs-ICG@rGO-DOX was finally employed for sequentially PTT with the combination of above obtained synergistic CLT and CT treatment for HT-29 cells to achieve the highest therapeutic efficiency from a single nanohybrid material by induce local hyperthermia upon NIR laser light exposure (808 nm, CW, 2 W/cm²). The dark toxicity of used NIR laser light intensity (2 W/cm²) and exposure time (0−30 min) was checked first in HT-29 cells by MTT assay and no obvious toxicity was obtained under these conditions, suggested the safer use of NIR laser (Figure S12a). However, when HT-29 cells were incubated with GNRs-ICG@rGO-DOX (300 μg/mL) for 24 h (cell viability at this stage ∼33% due to CLT and CT) and then followed by further NIR laser irradiation, the relative cell viability was reached up to 9.1% with time dependent manner under exposure of identical laser power intensity (Figure 5a, green line with hexagon symbol). The phenomena were attributed to the additional PTT effect from the nanohybrid under NIR light exposure. The effectiveness of CLT, CT, and PTT were further confirmed through the costaining of HT-29 cells by Calcein-AM and PI to visually distinguish live (green) and dead (red) cells,[43] respectively, before and after the various combination of treatments. As shown in Figure 5c, parts i and ii, any kind of cell death was not found in the case of the groups treated as control and with GNRs-ICG, which could be seen by the generation of only green fluorescence from live cells. The DOX only group was also shown in Figure 5c, part iii, in which green fluorescence along with some obvious red fluorescence from the dead cells were found to be observed for the anticancer property of DOX. However, a significant number of dead cells as red fluorescence was noticed in the case of incubated with GNRs-ICG@rGO under similar condition (Figure 5c, (iv). Furthermore, the cell ablation effect was additional improved by the treatment of GNRs-ICG@rGO-DOX (Figure 5c, (v) and GNRs-ICG@rGO-DOX followed by the guidance of NIR light irradiation (Figure 5c, part vi), which was reflected by the generation of a greater amount of red colored fluorescence by the dead cells. The live−dead cells staining results was successfully supported by the MTT cell viability tests. In the case of border applicability, the in vitro cellular imaging and combined therapeutics were also conducted toward another cancer cell line (HeLa, cervical cancer cells) and comparable results were also obtained as that of HT-29 cells (Figure S13). Therefore, the all over in vitro cell damage of cancer cells indicated that the nanohybrid materials is effective enough for tumor killing by the pathway of combination CLT with CT followed by sequential PTT and could make the GNRs-ICG@rGO-DOX as a treasured material for in vivo tumor treatment.[5]

The biodegradation behavior of GNRs-ICG@rGO-DOX was also determined for further potential clinical translation. It was evaluated by incubating the GNRs-ICG@rGO-DOX in PBS medium in acidic condition (pH ∼ 5.4) for several days and the morphology change was monitored by capturing the TEM images (Figure S14). It was noticed that the morphology was eventually started to collapse after 2 day of incubation and significantly collapsed after 7 days, and only individual GNRs existed.

In Vivo Image-Guided Tumor Therapeutics. After successful demonstration of in vitro cellular localization and combined therapeutics for tumor treatment, we finally investigated the in vivo image guided cancer therapeutic efficiency by the GNRs-ICG@rGO-DOX nanohybrid. The HT-29 human colon cancer tumor bearing nude mice were peritumorally injected with 400 μg/mice of GNRs-ICG@rGO-DOX@Cy-5.5. At first, the in vivo distribution, particularly in the tumor region of GNRs-ICG@rGO-DOX@Cy-5.5 was
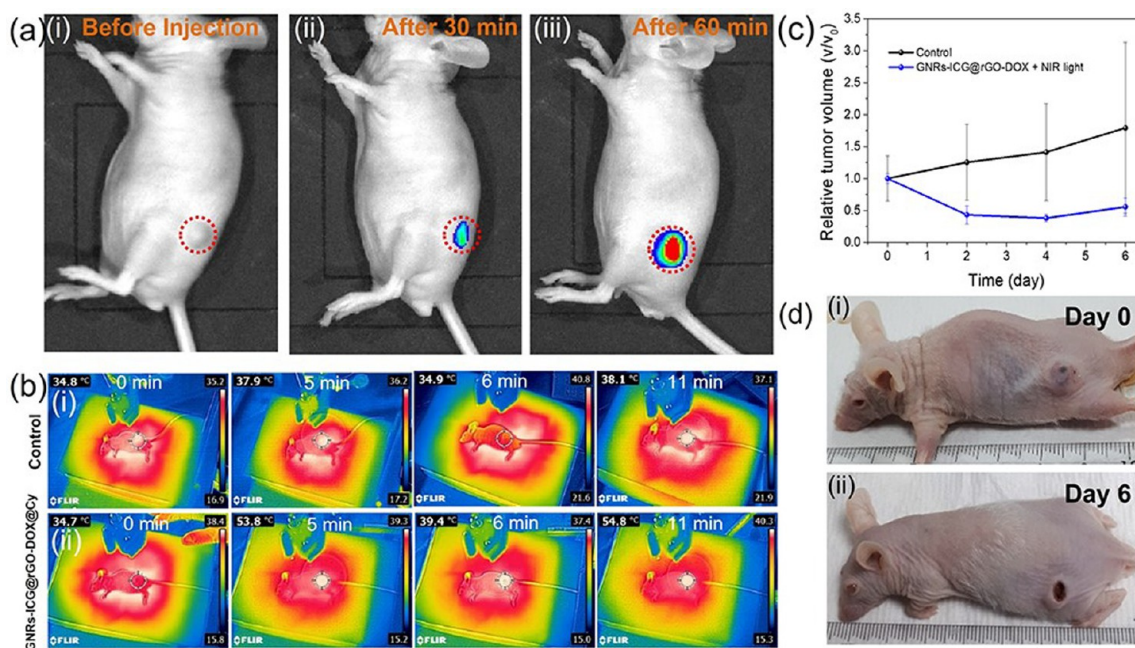
Figure 6. *In Vivo* imaging and triple-mode therapeutic performance. (a) The real-time NIR fluorescence images of a nu/nu mice (i) before and after (ii) 30 and (iii) 60 min of peritumoral injection of GNRs-ICG@rGO-DOX@Cy-5.5 (400 μg/mice) (λ_{ex} = 645 nm, λ_{ex} = 710 nm). The red dashed circles are the location of the grown tumor. (b) *In vivo* whole-body infrared thermal images of the HT-29 bearing nude mice at 0, 5, 6, and 11 min (i) as control and (ii) after peritumoral injection of GNRs-ICG@rGO-DOX@Cy-5.5 and 808 nm laser exposure (CW, 2 W/cm^2). (c) Time-dependent tumor volume changes for HT-29 tumors bearing mice within 6 days as control and peritumoral injection of GNRs-ICG@rGO-DOX@Cy-5.5 with 808 nm laser exposure (CW, 2 W/cm^2). (d) Representative photographs of the HT-29 tumor bearing mice (i) before and (ii) after the combined treatment (CLT, CT and PTT) with the GNRs-ICG@rGO-DOX@Cy-5.5 and 808 nm laser exposure (CW, 2 W/cm^2).

determined through NIR fluorescence imaging of the Cy-5.5 dye (λ_{ex} = 640 nm, λ_{ex} = 710 nm).[54] After injection of 30 min, a significantly observable fluorescence signal was detected in the tumor region (Figure 6a, part ii), which was became stronger with over time of 60 min (Figure 6a, part iii), as Cy-5.5 could be released in acidic condition. Thus, the tumor location could easily be identified in live mice through the NIR fluorescent imaging system with the use of GNRs-ICG@rGO-DOX@Cy-5.5 hybrid material. Therefore, with the NIR fluorescent image monitoring, it could be easier to monitor the tumor ablation effects in real time for accurate trimode therapy of HT-29 tumor bearing mice. The *in vivo* photo-thermal images were also captured by an infrared thermal camera to monitor the thermal imaging potentiality and PTT effects by the GNRs-ICG@rGO-DOX hybrid under 808 nm laser irradiation. For avoiding probable tissue injury by hyperthermia, the laser irradiation treatment was conducted for a total of 10 min with a lower power density of 2 W/cm^2 with 1 min interval after 5 min of laser exposure. As shown in Figure 6b, part ii, the surface temperature of the HT-29 bearing tumor was increased from 34.7 to 53.8 °C within 5 min of laser irradiation and further reached 54.8 °C at the time of 10 min laser irradiation, which is capable enough for killing the cancer cells. However, with PBS injection, only 3.3 °C temperature increase was observed for the control experiment (Figure 6b, part i).[23] The relative change in temperature of the tumor surface with the laser irradiation time (from 0 to 5 min with 1 min intervals) is also shown in Figure S15. The epidermis was not burnt throughout the laser irradiation process on the conscious mice and the temperature quickly decayed to the body temperature after a 1 min turn off of the laser source, suggesting it as a safer treatment.

The exciting *in vitro* outcomes of high biocompatibility/biodegradability with enhanced combination therapeutic efficacy of GNRs-ICG@rGO-DOX nanohybrid thus may suggest to us a hypothetically improved *in vivo* therapeutic performance. To verify this phenomenon, the therapeutic efficacy was examined on HT-29 human colon cancer tumor xenograft on specific nude mice via peritumoral injections of GNRs-ICG@rGO-DOX nanohybrid and under different treatment conditions. PBS as a control group was also administrated peritumorally to compare the therapeutic efficiency. The body weights of mice in control and in the case of the therapeutic group did not demonstrate any significant change during 4 days of the therapeutic period, which supported no significant toxicity by the injection of GNRs-ICG@rGO-DOX during the treatment period.[42−44] In the case of the *in vivo* tumor suppression assessments, we only performed the combined therapeutic mode, i.e., CLT with CT followed by the PTT mode of therapeutics, since the *in vitro* combined triple-mode of therapeutics was the most efficient performance by the GNRs-ICG@rGO-DOX nanohybrid (Figures 5 and S13) and also due to the limited facility of extensive *in vivo* experiments. As shown in Figure 6c, compared to that of control experiment condition (black line), the peritumoral administration of GNRs-ICG@rGO-DOX followed by the NIR laser irradiation gave us satisfactory suppression effects (Figure 6c, blue line) and to be more specific, by considering the relative tumor volume suppression rates of ∼44.0%, at a dose administration of 400 μg/mouse. The antitumor efficacies also measured quantitatively by calculating the variation of tumor weights and similar results was found, whereas no obvious tumor cell damage was obtained in the case of control one. The visually demonstration of the mice before and after the therapeutic processes are

shown in Figure 6d, in which the clear evidence for the effective reduction of the HT-29 tumor size and growth was noticed. Thus, the above-mentioned *in vitro* and *in vivo* outcomes proposed that HT-29 tumor growth could be effectively suppressed by the administration of GNRs-ICG@rGO-DOX hybrid material under 808 nm laser irradiation by the combination of (i) catalytic therapy through the generation of excess ROS in tumor site, which leads to mitochondria-mediated apoptosis; (ii) chemotherapy by prompting cell apoptosis using anticancer drug DOX; and (iii) photothermal therapy techniques.

CONCLUSION

In conclusion, we have grown a newer kind of hybrid material for the first time consisting of plasmonic nanostructures (GNRs), mesoporous silica, dyes (ICG and Cy-5.5), and drug (DOX) with a 2-D graphene. The GNRs-ICG@rGO-DOX nanohybrid system (width ∼60 nm and length ∼90 nm) was found to be remarkably stable under physiological conditions and showed excellent biocompatible with admirable biodegradability in an acidic situation. The hybrid material has a suitable NIR absorption (∼780 nm) capability in the biological window of tumor detection and therapy along with three remarkable capabilities of nanozymatic activity, drug carrier ability, and photothermal activity. The *in vitro* and *in vivo* NIR fluorescence imaging technique was adopted for diagnosis of the HT-29 tumor. Then, combined catalytic and chemo-therapeutic performance with combinatorial photothermal therapeutic activity have been demonstrated for competent tumor growth destruction by our designed multifunctional nanohybrid design. Thus, the integration of multimodal techniques into a single nanoplatform allows for effective tumor therapy contemporarily with improved tumor specificity and minimal side effects to normal organs/tissues, which holds attractive promises for further development in cancer therapy.

ASSOCIATED CONTENT

Ⓢ Supporting Information

The Supporting Information is available free of charge at https://pubs.acs.org/doi/10.1021/acsomega.2c01306.

> Additional supporting data such as in details experiments methods, additional characterization of nanomaterials, and additional supporting experiments (PDF)

AUTHOR INFORMATION

Corresponding Authors

Dong Ha Kim — *Department of Chemistry and Nano Science, Ewha Womans University, Seoul 03760, Republic of Korea;* ⓞ orcid.org/0000-0003-0444-0479; Email: dhkim@ewha.ac.kr

Hyukjin Lee — *College of Pharmacy, Graduate School of Pharmaceutical Sciences, Ewha Womans University, Seoul 03760, Republic of Korea;* ⓞ orcid.org/0000-0001-9478-8473; Email: hyukjin@ewha.ac.kr

Sehoon Kim — *Chemical and Biological Integrative Research Center, Korea Institute of Science and Technology, Seoul 02792, Republic of Korea; KU-KIST Graduate School of Converging Science and Technology, Korea University, Seoul 02841, Republic of Korea;* ⓞ orcid.org/0000-0002-8074-1006; Email: sehoonkim@kist.re.kr

Authors

Swarup Kumar Maji — *Department of Chemistry, Khatra Adibasi Mahavidyalaya, Khatra 722140 West Bengal, India; Department of Chemistry and Nano Science, Ewha Womans University, Seoul 03760, Republic of Korea;* ⓞ orcid.org/0000-0003-3282-3397

Subin Yu — *Department of Chemistry and Nano Science, Ewha Womans University, Seoul 03760, Republic of Korea;* ⓞ orcid.org/0000-0002-8791-2277

Eunshil Choi — *Chemical and Biological Integrative Research Center, Korea Institute of Science and Technology, Seoul 02792, Republic of Korea*

Ju Won Lim — *Department of Chemistry and Nano Science, Ewha Womans University, Seoul 03760, Republic of Korea;* ⓞ orcid.org/0000-0001-7021-3173

Dohyub Jang — *Chemical and Biological Integrative Research Center, Korea Institute of Science and Technology, Seoul 02792, Republic of Korea; Department of Biomicrosystem Technology, 145 Anam-ro, Seongbuk-gu, Korea University, Seoul 02841, Republic of Korea;* ⓞ orcid.org/0000-0003-1037-544X

Ga-young Kim — *Chemical and Biological Integrative Research Center, Korea Institute of Science and Technology, Seoul 02792, Republic of Korea*

Complete contact information is available at:
https://pubs.acs.org/10.1021/acsomega.2c01306

Author Contributions

The paper was completed by contributions of all of the authors. All of the authors approved the final version of the paper.

Notes

The authors declare no competing financial interest.

ACKNOWLEDGMENTS

REFERENCES

(1) Chen, G.; Roy, I.; Yang, C.; Prasad, P. N. Nanochemistry and Nanomedicine for Nanoparticle-Based Diagnostics and Therapy. *Chem. Rev.* **2016**, *116*, 2826−2885.

(2) Ryu, J. H.; Koo, H.; Sun, I.-C.; Yuk, S. H.; Choi, K.; Kim, K.; Kwon, I. C. Tumor-Targeting Multi-Functional Nanoparticles for Thernostics: New Paradigm for Cancer Therapy. *Adv. Drug Delivery Rev.* **2012**, *64*, 1447−1458.

(3) Mura, S.; Couvreur, P. Nanotheranostics for Personalized Medicine. *Adv. Drug Delivery Rev.* **2012**, *64*, 1394−1416.

(4) Menon, J. U.; Jadeja, P.; Tambe, P.; Vu, K.; Yuan, B.; Nguyen, K. T. Nanomaterials for Photo-Based Diagnostic and Therapeutic Applications. *Theranostics* **2013**, *3*, 152−166.

(5) Fan, W.; Yung, B.; Huang, P.; Chen, X. Nanotechnology for Multimodal Synergistic Cancer Therapy. *Chem. Rev.* **2017**, *117*, 13566−13638.

(6) Zheng, J.; Cheng, X.; Zhang, X.; Bai, X.; Ai, R.; Shao, L.; Wang, J. Gold Nanorods: The Most Versatile Plasmonic Nanoparticles. *Chem. Rev.* **2021**, *121*, 13342−13453.

(7) Cobley, C. M.; Chen, J.; Cho, E. C.; Wang, L. V.; Xia, Y. Gold Nanostructures: A Class of Multifunctional Materials for Biomedical Applications. *Chem. Soc. Rev.* **2011**, *40*, 44−56.

(8) Wang, H.; Huff, T. B.; Zweifel, D. A.; He, W.; Low, P. S.; Wei, A.; Cheng, J. X. In Vitro and In Vivo Two-Photon Luminescence Imaging of Single Gold Nanorods. *Proc. Natl. Acad. Sci. U. S. A.* **2005**, *102*, 15752−15756.

(9) Durr, N. J.; Larson, T.; Smith, D. K.; Korgel, B. A.; Sokolov, K.; Ben-Yakar, A. Two-photon Luminescence Imaging of Cancer Cells using Molecularly Targeted Gold Nanorods. *Nano Lett.* **2007**, *7*, 941−945.

(10) Jung, Y.; Reif, R.; Zeng, Y.; Wang, R. K. Three-Dimensional High-Resolution Imaging of Gold Nanorods Uptake in Sentinel Lymph Nodes. *Nano Lett.* **2011**, *11*, 2938−2943.

(11) Nguyen, V.-P.; Li, Y.; Henry, J.; Zhang, W.; Wang, X.; Paulus, Y. M. Gold Nanorod Enhanced Photoacoustic Microscopy and Optical Coherence Tomography of Choroidal Neovascularization. *ACS Appl. Mater. Interfaces* **2021**, *13*, 40214−40228.

(12) Ye, Z.; Li, C.; Celentano, M.; Lindley, M.; O'Reilly, T.; Greer, A. J.; Huang, Y.; Hardacre, C.; Haigh, S. J.; Xu, Y.; Bell, S. E. J. Surfactant-free Synthesis of Spiky Hollow Ag−Au Nanostars with Chemically Exposed Surfaces for Enhanced Catalysis and Single-Particle SERS. *JACS Au* **2022**, *2*, 178−187.

(13) Lin, Y.; Zhao, M.; Guo, Y.; Ma, X.; Luo, F.; Guo, L.; Qiu, B.; Chen, G.; Lin, Z. Multicolor Colormetric Biosensor for the Determination of Glucose Based on the Etching of Gold Nanorods. *Sci. Reports* **2016**, *6*, 37879.

(14) Li, C.; Feng, K.; Xie, N.; Zhao, W.; Ye, L.; Chen, B.; Tung, C.-H.; Wu, L.-Z. Mesoporous Silica-Coated Gold Nanorods with Designable Anchor Peptides for Chemo-Photothermal Cancer Therapy. *ACS Appl. Nano Mater.* **2020**, *3*, 5070−5078.

(15) Ke, H.; Wang, J.; Dai, Z.; Jin, Y.; Qu, E.; Xing, Z.; Guo, C.; Yue, X.; Liu, J. Gold-Nanoshelled Microcapsules: A Theranostic Agent for Ultrasound Contrast Imaging and Photothermal Therapy. *Angew. Chem., Int. Ed.* **2011**, *50*, 3017−3021.

(16) Slowing, I. I.; Vivero-Escoto, J. L.; Wu, C. W.; Lin, V. Mesoporous Silica Nanoparticles as Controlled Release Drug Delivery and Gene Transfection Carriers. *Adv. Drug Deliv Rev.* **2008**, *60*, 1278−1288.

(17) Wijaya, A.; Schaffer, S. B.; Pallares, I. G.; Hamad-Schifferli, K. Selective Release of Multiple DNA Oligonucleotides from Gold Nanorods. *ACS Nano* **2009**, *3*, 80−86.

(18) Wu, B.; Liu, D.; Mubeen, S.; Chuong, T. T.; Moskovits, M.; Stucky, G. D. Anisotropic Growth of TiO₂ onto Gold Nanorods for Plasmon-Enhanced Hydrogen Production from Water Reduction. *J. Am. Chem. Soc.* **2016**, *138*, 1114−1117.

(19) Wang, C.; Astruc, D. Nanogold Plasmonic Photocatalysis for Organic Synthesis and Clean Energy Conversion. *Chem. Soc. Rev.* **2014**, *43*, 7188−7216.

(20) Zijlstra, P.; Chon, J. W. M.; Gu, M. Five-Dimensional Optical Recording Mediated by Surface Plasmons in Gold Nanorods. *Nature* **2009**, *459*, 410−413.

(21) Zhang, Q.; Xia, Z.; Cheng, Y. B.; Gu, M. High-Capacity Optical Long Data Memory Based on Enhanced Young's Modulus in Nanoplasmonic Hybrid Glass Composites. *Nat. Commun.* **2018**, *9*, 1183.

(22) Zhang, Z.; Wang, L.; Wang, J.; Jiang, X.; Li, X.; Hu, Z.; Ji, Y.; Wu, X.; Chen, C. Mesoporous Silica-Coated Gold Nanorods as a Light-Mediated Multifunctional Theranostic Platform for Cancer Treatment. *Adv. Mater.* **2012**, *24*, 1418−1423.

(23) Li, Y.; Wen, T.; Zhao, R.; Liu, X.; Ji, T.; Wang, H.; Shi, X.; Shi, J.; Wei, J.; Zhao, Y.; Wu, X.; Nie, G. Localized Electric Field of Plasmonic Nanoplatform Enhanced Photodynamic Tumor Therapy. *ACS Nano* **2014**, *8*, 11529−11542.

(24) Stewart, M. E.; Anderton, C. R.; Thompson, L. B.; Maria, J.; Gray, S. K.; Rogers, J. A.; Nuzzo, R. G. Nanostructured Plasmonic Sensors. *Chem. Rev.* **2008**, *108*, 494−521.

(25) Tong, L.; Wei, Q.; Wei, A.; Cheng, J. X. Gold Nanorods as Contrast Agents for Biological Imaging: Optical Properties, Surface Conjugation and Photothermal Effects. *Photochem. Photobiol.* **2009**, *85*, 21−32.

(26) Alkilany, A. M.; Thompson, L. B.; Boulos, S. P.; Sisco, P. N.; Murphy, C. J. Gold Nanorods: Their Potential for Photothermal Therapeutics and Drug Delivery, Tempered by the Complexity of their Biological Interactions. *Adv. Drug Delivery Rev.* **2012**, *64*, 190−199.

(27) Luo, S.; Zhang, E.; Su, Y.; Cheng, T.; Shi, C. A Review of NIR Dyes in Cancer Targeting and Imaging. *Biomaterials* **2011**, *32*, 7127−7138.

(28) Chen, Y.; Chen, G.; Zhao, Y.; Wang, W. Indocyanine Green-Loaded Nanocarriers as Contrast Agents for NIR Fluorescent Optical Imaging. *J. Nanomed. Nanotechol.* **2012**, *03*, 122.

(29) Peng, D.; Du, Y.; Shi, Y.; Mao, D.; Jia, X.; Li, H.; Zhu, Y.; Wang, K.; Tian, J. Precise Diagnosis in Different Scenarios using Photoacoustic and Fluorescence Imaging with Dual-Modality Nano-particles. *Nanoscale* **2016**, *8*, 14480−14488.

(30) Bardhan, R.; Chen, W.; Bartels, M.; Perez-Torres, C. P.; Botero, M. F.; McAninch, R. W.; Contreras, A.; Schiff, R.; Pautler, R. G.; Halas, N. J.; Joshi, A. Tracking of Multimodal Therapeutic Nanocomplexes Targeting Breast Cancer in Vivo. *Nano Lett.* **2010**, *10*, 4920−4928.

(31) Luo, T.; Huang, P.; Gao, G.; Shen, G.; Fu, S.; Cui, D.; Zhou, C.; Ren, Q. Mesoporous Silica-Coated Gold Nanorods with Embedded Indocyanine Green for Dual Mode X-ray CT and NIR Fluorescence Imaging. *Opt. Express* **2011**, *19*, 17030−17039.

(32) Zeng, C.; Shang, W.; Liang, X.; Liang, X.; Chen, Q.; Chi, C.; Du, Y.; Fang, C.; Tian, J. Cancer Diagnosis and Imaging-Guided Photothermal Therapy Using a Dual-Modality Nanoparticle. *ACS Appl. Mater. Interfaces* **2016**, *8*, 29232−29241.

(33) Yin, P. T.; Shah, S.; Chhowalla, M.; Lee, K. B. Design, Synthesis, and Characterization of Graphene-Nanoparticle Hybrid Materials for Bioapplications. *Chem. Rev.* **2015**, *115*, 2483−2531.

(34) Ma, X.; Qu, Q. Y.; Zhao, Y.; Luo, Z.; Zhao, Y.; Ng, K. W.; Zhao, Y. Graphene Oxide Wrapped Gold Nanoparticles for Intracellular Raman Imaging and Drug Delivery. *J. Mater. Chem. B* **2013**, *1*, 6495−6500.

(35) Lin, H.; Chen, Y.; Shi, J. Nanoparticle-Triggered In Situ Catalytic Chemical Reactions for Tumour-Specific Therapy. *Chem. Soc. Rev.* **2018**, *47*, 1938−1958.

(36) Gorelikov, I.; Matsuura, N. Single-Step Coating of Mesoporous Silica on Cetyltrimethyl Ammonium Bromide-Capped Nanoparticles. *Nano Lett.* **2008**, *8*, 369−373.

(37) Johnson, P. B.; Christy, R. W. Optical Constants of Noble Metals. *Phys. Rev. B: Solid State* **1972**, *6*, 4370−4379.

(38) Yang, K.; Feng, L.; Hong, H.; Cai, W.; Liu, Z. Preparation and Functionalization of Graphene Nanocomposites for Biomedical Applications. *Nat. Protocols* **2013**, *8*, 2392−2403.

(39) Sreejith, S.; Joseph, J.; Nguyen, K. T.; Murukeshan, V. M.; Lye, S. W.; Zhao, Y. Graphene Oxide Wrapping of Gold−Silica Core−Shell Nanohybrids for Photoacoustic Signal Generation and Bimodal Imaging. *ChemNanoMat* **2015**, *1*, 39−45.

(40) Ferrauto, G.; Carniato, F.; Di Gregorio, E.; Tei, L.; Botta, M.; Aime, S. Large Photoacoustic Effect Enhancement for ICG Confined inside MCM-41 Mesoporous Silica Nanoparticles. *Nanoscale* **2017**, *9*, 99−103.

(41) Maji, S. K.; Mandal, A. K.; Nguyen, K. T.; Borah, P.; Zhao, Y. Cancer Cell Detection and Therapeutics using Peroxidase-Active Nanohybrid of Gold Nanoparticle-Loaded Mesoporous Silica-Coated Graphene. *ACS Appl. Mater. Interfaces* **2015**, *7*, 9807−9816.

(42) Fan, K.; Xi, J.; Fan, L.; Wang, P.; Zhu, C.; Tang, Y.; Xu, X.; Liang, M.; Jiang, B.; Yan, X.; Gao, L. In Vivo Guiding Nitrogen-Doped Carbon Nanozyme for Tumor Catalytic Therapy. *Nat. Commun.* **2018**, *9*, 1440.

(43) Huo, M.; Wang, L.; Chen, Y.; Shi, J. Tumor-Selective Catalytic Nanomedicine by Nanocatalyst Delivery. *Nat. Commun.* **2017**, *8*, 357.

(44) Wang, Z.; Zhang, Y.; Ju, E.; Liu, Z.; Cao, F.; Chen, Z.; Ren, J.; Qu, X. Biomimetic Nanoflowers by Self-Assembly of Nanozymes to Induce Intracellular Oxidative Damage against Hypoxic Tumors. *Nat. Commun.* **2018**, *9*, 3334.

(45) Cao, F.; Zhang, Y.; Sun, Y.; Wang, Z.; Zhang, L.; Huang, Y.; Liu, C.; Liu, Z.; Ren, J.; Qu, X. Ultrasmall Nanozymes Isolated within Porous Carbonaceous Frameworks for Synergistic Cancer Therapy: Enhanced Oxidative Damage and Reduced Energy Supply. *Chem. Mater.* **2018**, *30*, 7831−7839.

(46) Maji, S. K.; Yu, S.; Chung, K.; Sekkarapatti Ramasamy, M.; Lim, J. W.; Wang, J.; Lee, H.; Kim, D. H. Synergistic Nanozymetic Activity of Hybrid Gold Bipyramid−Molybdenum Disulfide Core@ Shell Nanostructures for Two-Photon Imaging and Anticancer Therapy. *ACS Appl. Mater. Interfaces* **2018**, *10*, 42068−42076.

(47) Hu, D.; Zhang, J.; Gao, G.; Sheng, Z.; Cui, H.; Cai, L. Indocyanine Green-Loaded Polydopamine-Reduced Graphene Oxide Nanocomposites with Amplifying Photoacoustic and Photothermal Effects for Cancer Theranostics. *Theranostics* **2016**, *6*, 1043−1052.

(48) Xu, C.; Yang, D.; Mei, L.; Li, Q.; Zhu, H.; Wang, T. Targeting Chemophotothermal Therapy of Hepatoma by Gold Nanorods/ Graphene Oxide Core/Shell Nanocomposites. *ACS Appl. Mater. Interfaces* **2013**, *5*, 12911−12920.

(49) Taylor, K.; Tabish, T. A.; Narayan, R. Drug Release Kinetics of DOX-Loaded Graphene-Based Nanocarriers for Ovarian and Breast Cancer Therapeutics. *J. Appl. Sci.* **2021**, *11*, 11151.

(50) Kuo, W. S.; Chang, Y. T.; Cho, K. C.; Chiu, K. C.; Lien, C. H.; Yeh, C. S.; Chen, S. J. Gold Nanomaterials Conjugated with Indocyanine Green for Dual-Modality Photodynamic and Photo-thermal Therapy. *Biomaterials* **2012**, *33*, 3270−3278.

(51) Fiorillo, M.; Verre, A. F.; Iliut, M.; Peiris-Pagés, M.; Ozsvari, B.; Gandara, R.; Cappello, A. R.; Sotgia, F.; Vijayaraghavan, A.; Lisanti, M. P. Graphene Oxide Selectively Targets Cancer Stem Cells, Across Multiple Tumor Types: Implications for Non-Toxic Cancer Treat-ment, via "Differentiation-based Nano-Therapy. *Oncotarget* **2015**, *6*, 3553−3562.

(52) Mittal, S.; Kumar, V.; Dhiman, N.; Chauhan, L. K. S.; Pasricha, R.; Pandey, A. K. Physico-Chemical Properties based Differential Toxicity of Graphene Oxide/Reduced Graphene Oxide in Human Lung Cells Mediated Through Oxidative Stress. *Sci. Reports* **2016**, *6*, 39548.

(53) Lammel, T.; Boisseaux, P.; Fernández-Cruz, M. L. F.; Navas, J. M. Internalization and Cytotoxicity of Graphene Oxide and Carboxyl Graphene Nanoplatelets in the Human Hepatocellular Carcinoma Cell Line HepG2. *Particle and Fibre Toxicology* **2013**, *10*, 27.

(54) Zhang, F.; Cao, J.; Chen, X.; Yang, K.; Zhu, L.; Fu, G.; Huang, X.; Chen, X. Noninvasive Dynamic Imaging of Tumor Early Response to Nanoparticle-mediated Photothermal Therapy. *Theranostics* **2015**, *5*, 1444−1455.